Astronomy & Astrophysics manuscript no. aa55157-25
June 23, 2025

Tales of stellar and binary co-evolution, told by stellar oscillations

Binary demographics and their impact on stellar mass, orbits, and age estimates in main-sequence and red-giant stars

Paul G. Beck

[1] Instituto de Astrofísica de Canarias, E-38200 La Laguna, Tenerife, Spain; e-mail: paul.beck@iac.es, paul.beck@gmx.at
[2] Departamento de Astrofísica, Universidad de La Laguna, E-38206 La Laguna, Tenerife, Spain

Submitted: April 14, 2025

ABSTRACT

Context. Red giants are increasingly used as stellar population tracers due to their well-understood evolution and the availability of asteroseismic observables. However, stellar binarity can alter observable properties and introduce strong biases.
Aims. Assessing a holistic picture of the binary population and evolution in the red giant phase through characterizing the sample of binaries hosting oscillating red-giant stars from the combination of large asteroseismic, spectroscopic, and astrometric surveys.
Methods. We investigate the binary properties of evolved stars in the APOKASC 3 and APO-K2 catalogs, leveraging asteroseismic constraints and *Gaia* DR3 non-single-star solutions. We explore the mass distribution of red-giant binary systems, analyze the evolution of their binary fraction. We investigate the impact of stellar evolution on the orbital periods ($P_{\rm orb}$), eccentricities, radial velocity amplitudes and the fractional radius and identify candidate systems that may have undergone significant interactions.
Results. For stars with $M \leq 1.8 M_{\odot}$, we find binary fractions ~31% and ~41% for oscillating and non-oscillating solar-like stars on the main-sequence (MS). By using the peak frequency of the oscillation power excess ($\nu_{\rm max}$) as luminosity proxy and evolutionary states, we detect a binary attrition of ~69% and ~81% on the low- and high-luminosity red-giant branch (RGB) and an additional ~38% to the red clump (RC), with respect to the MS. Binaries hosting RC and secondary clump stars (2RC) stars are largely depleted at $P_{\rm orb} \lesssim 500$ and $\lesssim 200$ days, respectively. We identify a population of rapidly rotating RC stars in short-period orbits as potential post-common-envelope merger products. Mass-dependent differences in binary fractions and orbital properties point to stronger binary attrition for stars with $M \leq 1.8\,M_{\odot}$.
Conclusions. Binarity is not the primary cause of reduced oscillation amplitudes in main-sequence solar-like stars. The distinct mass distributions and depletion of short-period binaries in the red-giant phase underscore the impact of stellar expansion and binary interaction on stellar evolution. RC systems with $P_{\rm orb} \lesssim 800$ to 1,000 days are likely shaped by past interactions, such as mass transfer or loss, which can lead to significantly biased age estimates if not accounted for. This demonstrates the importance of identifying stellar binarity when using red giants as population tracers.

Key words. Asteroseismology – (Stars:) binaries: spectroscopic – Stars: late-type – Stars: oscillations (including pulsations).

1. Introduction

Understanding how stars evolve in binary systems is crucial for building a holistic picture of the co-evolution of stars as well as of the evolution of a binary as a whole. Binary systems are formed in a wide range of orbital periods and eccentricities, leading to diverse evolutionary pathways depending on the initial masses, separations, and interactions between the components (Offner et al. 2023; Moe & Di Stefano 2017, and references therein). A star's internal structure, which is governed by its mass and evolutionary stage (Salaris & Cassisi 2005; Kippenhahn et al. 2013; Pinsonneault & Ryden 2023), dictates how it responds to binary interactions (Zahn 1977, 2013; Ogilvie 2013; Esseldeurs et al. 2024). This interplay not only influences the evolution of the individual stars but also shapes the orbital architecture and the ultimate fate of the system as a whole.

Unless formed through a rare capturing event, binary stars are generally coeval, having formed from the same molecular cloud (Offner et al. 2023), justifying the assumption of an identical initial chemical composition (Torres et al. 2010). Therefore, the ages its stellar components are typically assumed to be similar, within the free-fall time of the star-forming filament of the interstellar cloud from which the binary system has emerged (Offner et al. 2023). At a common distance, differences in luminosity and color can be attributed to differences in evolutionary stage rather than interstellar extinction. With these shared characteristics, the key parameter that governs the disparity between the two components is their difference in mass, which can be accurately determined from the radial velocities (RV) solution of a double-lined spectroscopic binary (SB2) system. In particular, in the red-giant phase, mass ratios differing from unity by a few percent will lead to pronounced differences in the stellar evolution of the two components (Miglio et al. 2014; Beck et al. 2018a). Such systems are benchmarks for calibrating stellar models, testing complex physics, and validating model-dependent age estimates (del Burgo & Allende Prieto 2018; Beck et al. 2018a; Jørgensen et al. 2020; Grossmann et al. 2025).

About half of all solar-like stars (from late F, G, to early K; $0.8 \lesssim M/M_{\odot} \lesssim 1.5$) on the main sequence (MS) are members of binary or multiple systems (Lada 2006; Offner et al. 2023; Moe & Di Stefano 2017). However, the binary fraction and the distribution of orbital parameters evolve as the stars evolve. The most significant transformations occur during the red-giant branch

(RGB) and asymptotic-giant branch (AGB) phases, where the evolving star experience a dramatic expansion of their radii (e.g., Serenelli et al. 2017; Hekker et al. 2020). These changes can trigger complex interactions, such as tidal effects, mass transfer, and common-envelope evolution that substantially alter both, stellar and orbital properties (Ivanova et al. 2013). Based on stellar population synthesis, Mazzi et al. (2025) estimates that ∼1% of red giants observed by the NASA *Kepler* mission (Borucki et al. 2010) have undergone mass transfer episodes. Such interactions can rejuvenate a star or make it appear prematurely evolved, potentially biasing age estimates and affecting the inferred age-metallicity relation of the Galaxy (Mazzi et al. 2025).

Asteroseismology of solar-like oscillators has proven to be a powerful tool to characterize individual stars and stellar ensembles. Solar-like oscillations are stochastically excited by convective motions in the outer layers of stars and are observed from the main sequence through to the red-giant branch (e.g. Chaplin & Miglio 2013; Houdek & Dupret 2015, and references therein). Their frequencies are susceptible to the stellar structure, enabling the determination of key parameters such as mass, radius (Kjeldsen & Bedding 1995; Kallinger et al. 2010), and age (e.g., Creevey et al. 2017; Anders et al. 2023). The discovery of mixed modes (Beck et al. 2011; Bedding et al. 2011) extended the seismic analysis into the central regions of the star, allowing to determine the evolutionary state (Bedding et al. 2011; Mosser et al. 2014) and constrain the internal rotational gradient (Beck et al. 2012). Binary systems play an essential role in seismology for calibrating the scaling relations (Gaulme et al. 2016; Benbakoura et al. 2021) and testing stellar models (Grossmann et al. 2025; Schimak et al. 2025).

Thanks to continuous observations from NASA missions such as *Kepler*, K2 (Howell et al. 2014), and TESS (Transiting Exoplanet Survey Satellite; Ricker et al. 2014), and ESA's *Gaia* (Gaia Collaboration et al. 2016), a large and growing sample of solar-like oscillators in binary systems is now available. In particular, the Non-Single Star catalog (NSS; Gaia Collaboration et al. 2023a) from *Gaia* Data Release 3 (DR3; Gaia Collaboration et al. 2023b) has provided orbital solutions for approximately 500,000 systems, along with numerous binary indicators. This treasure trove of data offers unprecedented opportunities to investigate the mutual influence of binarity and stellar evolution in exquisite detail. By combining data from *Gaia*, *Kepler*, and TESS, Beck et al. (2022, 2024) significantly expanded the sample of known solar-like oscillators in binary systems across all evolutionary stages with detectable oscillations.

In this paper, we investigate the evolution of the binary fraction, orbital properties, and mass distribution of red-giant stars in binary systems by leveraging the combination of asteroseismic constraints and *Gaia* DR3 binary solutions. We analyze samples of oscillating red giants from the APOKASC 3 (Pinsonneault et al. 2025) and APO-K2 (Zinn et al. 2022) catalogs, supplemented with homogeneous spectroscopic parameters from APOGEE (Apache Point Observatory Galactic Evolution Experiment; Majewski et al. 2017) (Sect. 2). By cross-matching these samples with the NSS orbital solutions and binary indicators, we study how the binary fraction varies with stellar mass and evolutionary state (Sect. 3), and explore the impact of binarity on the red-giant mass distribution (Sect. 4). In Sect. 5, we examine the attenuation of radial velocity amplitudes, which may indicate common-envelope evolution or merger events. Our findings provide new empirical constraints on the co-evolution of stellar and orbital properties in binary systems hosting evolved stars. Conclusions are presented in Sect. 6.

2. Sample definition

Following the approach of Beck et al. (2022, 2024), we work under the hypothesis that the oscillating component is the more massive, primary component. The more massive primary evolves faster and is typically the brighter star during the H-shell burning phase of RGB. Because only the mode heights and not their frequencies are affected by photometric dilution, the presence of a secondary does not influence the determination of global parameters (Beck et al. 2018a; Sekaran et al. 2019). When another bright giant is present, the reduced signal-to-noise ratio will substantially increase the parameter uncertainty.

The assumption that the photometrically dominating star is the primary does not hold for systems where the primary has already reached the He-core burning red-clump phase, while the secondary still progresses on the RGB, probably more luminous than the primary. In such systems, the mass ratio may significantly deviate from the initial value due to increased mass loss at the RGB tip and even can be inverted (Schimak et al. 2025). Given the brief duration of the red-giant phase, such systems are expected to be rare (Miglio et al. 2014; Mazzi et al. 2025).

2.1. APOKASC 3 catalog

The APOKASC 3 catalog[1] by Pinsonneault et al. (2025) presents the final and most extensive compilation of the joint survey of asteroseismology of solar-like stars, combining data from the *Kepler* mission with consistent spectroscopy from APOGEE (for earlier versions, see APOKASC 1 and 2, in Pinsonneault et al. 2014, 2018, respectively). In its third iteration, the catalog provides mass and radius estimates for more than 12,000 red giants, with the excess of their oscillation power, $\nu_{\rm max}$, in the range $300 \gtrsim \nu_{\rm max}\,[\mu{\rm Hz}] \gtrsim 0.1$ (Fig. 1). For each star, values from APOGEE DR17 are available, providing a consistent set of fundamental spectroscopic parameters.

Stellar masses were derived from the asteroseismic scaling relations (Brown et al. 1991; Kjeldsen & Bedding 1995; Kallinger et al. 2010) for 10,036 stars, whose power spectral density allowed for reliable measurements of the global seismic parameters, which are the peak frequency of the oscillation's power excess, $\nu_{\rm max}$, and the large-frequency separation between consecutive radial orders, $\Delta\nu$. The obtained seismic parameters were corrected following the procedure of Mosser et al. (2012) to account for their departure from the regime of asymptotic oscillation theory. The stellar radii were calculated from the luminosity, using *Gaia* DR3 data (for details, see Zinn 2021).

APOKASC 3 presents the seismically inferred evolutionary state of the oscillating red giant based on the dipole-mixed-mode period-spacing measurements ($\Delta\Pi_1$) presented by Vrard et al. (2024). This parameter distinguishes the evolutionary phase, specifically RGB and He-core burning stars (Bedding et al. 2011; Mosser et al. 2014). However, the catalog does not discriminate between red-clump (RC) stars and more massive secondary-clump (2RC) stars, which both are in the phase of quiescent He-core burning but differ in whether helium ignition occurred under degenerate or non-degenerate conditions. In our analysis, we distinguish them based on their seismically inferred masses, using $1.8\,{\rm M}_\odot$ as the threshold. The color code in Fig. 1 discriminates between these three evolutionary states in the giant phase.

The distinction between RGB and AGB stars becomes increasingly uncertain for stars that are more luminous than the

[1] The APOKASC 3 catalog files are electronically available for download at https://zenodo.org/records/13308665

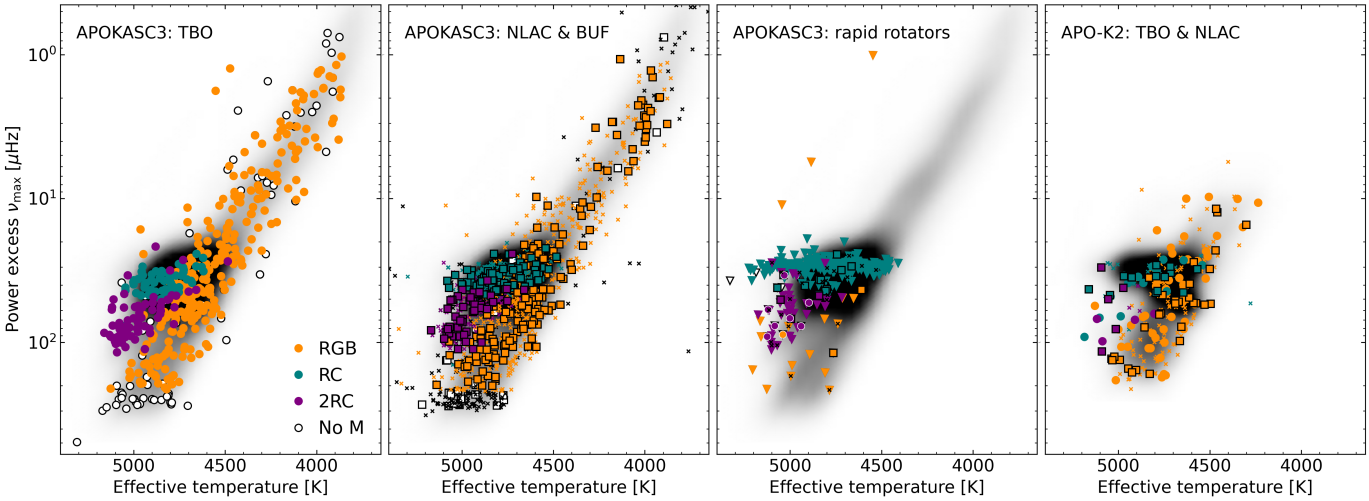

Fig. 1. Seismic Hertzsprung-Russell Diagrams of the investigated catalogs and binary samples. The two panels from left to right depict the targets in the APOKASC 3 catalog, with solutions in the *Gaia* catalogs of Two-Body Orbits (TBO) as dots and Non-Linear/Acceleration Solutions (NLAC) from NSS as squares. Additionally, the second panel shows the Binary Union Flag (x), which RUWE dominates. The third panel shows the stars with rapid surface rotation ($v \sin i \geq 5$ km/s) as triangles. Rapid-rotating targets found in binary systems are depicted as dots and squares or marked with crosses, depending on their solution type. The right panel presents TBO, NLAC, and RUWE binary indicators for targets in the APO-K2 catalog. The marker's surface color indicates its seismically determined evolutionary state, as indicated by the legend in the left panel; RGB: red-giant branch, RC: red clump, 2RC: secondary clump, No EvSt: no evolutionary state determined but mass reported, 'No M' indicates lower quality data that did not allow for a seismically inferred stellar mass. Stars with NLAC solutions are further marked with black edges.

RC. As noted by Pinsonneault et al. (2025), there is approximately a one-in-six chance that a star identified as being on the RGB is, in fact, on the AGB. Seismic discrimination between these two evolutionary phases remains challenging (Dréau et al. 2021). Following Pinsonneault et al. (2025), we treat AGB stars like RGB stars throughout our analysis. Using seismic parameters, inferred masses and evolutionary states were also used to obtain the stellar ages from comparison with single-star models.

For the 10,036 stars with high-quality asteroseismic solutions, the median fractional uncertainties in ν_{max} and $\Delta\nu$ are both 0.6%. The fractional uncertainties for the mass, radius, and age are 3.8%, 1.8%, and 11.1%, respectively. We adopt these parameters in our analysis as reported in Pinsonneault et al. (2025). The catalog includes an additional set of 1,624 stars with lower-quality data, but no asteroseismic solutions are provided for these stars. For completeness, we also searched these systems for indications of binarity.

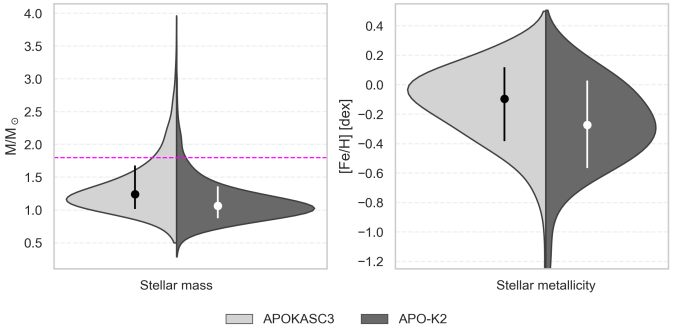

Fig. 2. Normalized kernel density estimates of the distributions for the stellar mass (left) and metallicity (right) for the APOKASC 3 (light) APO-K2 (dark) samples. The dots and vertical bars mark the respective sample's median and the interquartile range (25th–75th percentiles). The dashed magenta line indicates the mass threshold of 1.8 M$_\odot$.

2.2. APO-K2 catalog

The third version of the APO-K2 Catalog[2] by Zinn et al. (2022) presents a similarly comprehensive study, using APOGEE spectroscopy and asteroseismic detections of 7,673 oscillating red-giant stars from the Campaigns C1-C8 and C10-18 of the K2 mission. As this work has preceded *Gaia* DR3, it uses parallaxes from DR2 and a different correction method for the values of $\Delta\nu$. Furthermore, spectroscopic values from the APOGEE DR16 and GALAH DR2 are used. Due to the shorter time base and observational systematics of the K2 mission introduced by the satellite repositioning every ~6 hours, stars in the APO-K2 sample are found in a smaller range of oscillation frequencies, $200 \gtrsim \nu_{max}\,[\mu\text{Hz}] \gtrsim 5$ (Fig. 1). For this sample, the median fractional uncertainties in ν_{max} and $\Delta\nu$ are better than 2% and 1%, respectively. The fractional uncertainties for mass, radius, and age ~11%, ~7%, and ~20%, respectively.

The two samples appear to be significantly shifted when comparing the normalized kernel density estimates (KDE) of the stellar masses (Fig. 2), reported in the APOKASC 3 and the APO-K2 catalogs. However, the differences between the two works mentioned above only lead to slight variations. While the difference in parallax scale between DR2 and DR3 as well as the different correction of the scaling relations may introduce the most considerable shift, we argue that the leading cause is that K2 and *Kepler* sample stellar populations of different metallicities (Fig. 2), as the two missions probed different galactic latitudes (Fig. 3). A comparison done by Warfield et al. (2024) of the ages reported in the two samples found a good agreement when binning in distance to the Galactic plane. This finding suggests that this difference is due to a population effect but does not rule out a small systematic difference. Therefore, we treat the two samples separately.

[2] The APO-K2 catalog files are electronically available for download from CDS through the reference J/ApJ/926/191.

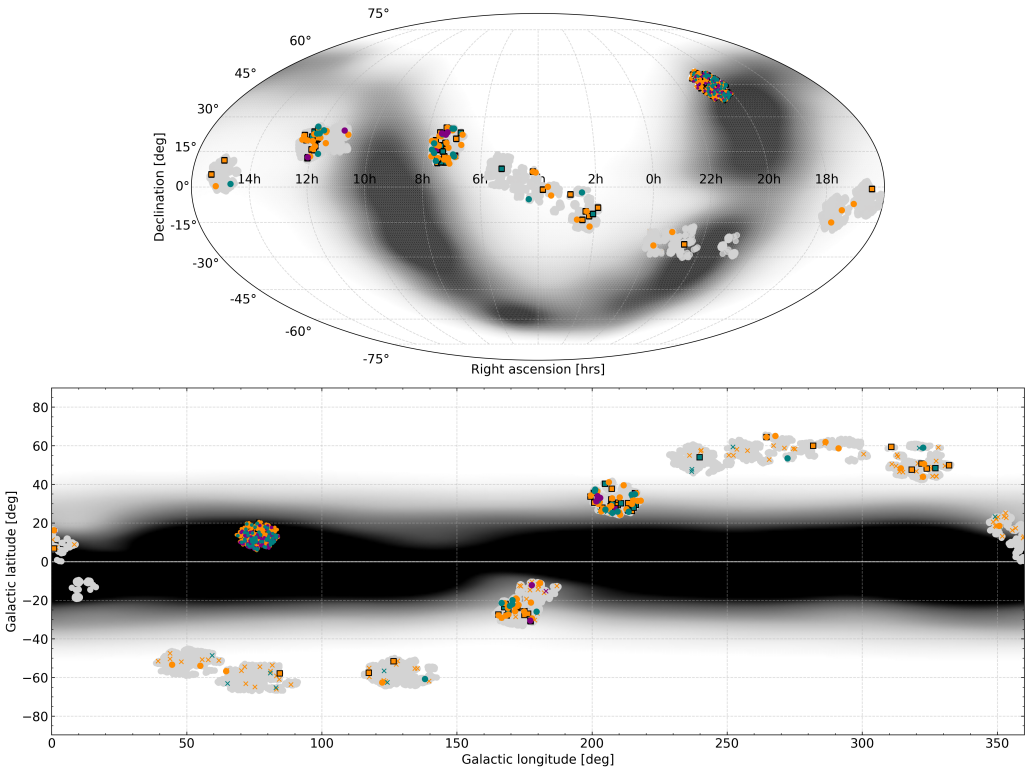

Fig. 3. Position of the observed samples on the equatorial plane of the sky (top panel) as well as in galactic coordinates (bottom panel). Grey data points indicate the position of the individual targets in the catalog with detected oscillations. The number of the K2 campaign (C) is given. The shape of the markers, representing various binary indicators and their colors indicating seismically inferred evolutionary states, are identical to Fig. 1. The color-shaded background depicts the distribution of all stars observed by *Gaia* with $G \leq 10$ mag.

2.3. Binary sample selection

As source of binarity indicators, we use the non-single-star catalog (NSS Gaia Collaboration et al. 2023a), published as part of the third data release (DR3) of the ESA *Gaia* mission (Gaia Collaboration et al. 2016, 2023b). It provides several sub-catalogs. First, we use the catalog of two-body orbit solutions (TBO), which presents about half a million orbital parameters derived from the RV time series, obtained with the *Gaia* Radial Velocity Spectrometer (RVS, Katz et al. 2023). Gaia Collaboration et al. (2023a) point out that these are binary candidates for which completeness was chosen over purity. From a detailed comparison of the SB9 catalog (Ninth Catalog of Spectroscopic Binary Orbits; Pourbaix et al. 2004), Beck et al. (2024) showed a good agreement for orbital periods $P_{orb} \lesssim 1{,}500$ days. We adopt a solution from the TBO as a binary candidate if at least the orbital period is provided in the catalog. For stars for which a single star model can not sufficiently explain the proper motion and no spectroscopic solution for an orbit was found, Gaia Collaboration et al. (2023a) provides non-linear or acceleration solutions (hereafter NLAC). The comparison with the SB9 confirmed that NLAC solutions indicate binaries with orbital periods typically much longer than 1,000 days (Beck et al. 2024).

An additional indicator of binarity from *Gaia* is the renormalized unit weight (RUWE). This quantity expresses the quality of the astrometric solution for a single star model. RUWE values larger than 1.4 are considered good indicators of unresolved binaries (Belokurov et al. 2020). However, even among the large sample of the SB9, ~40% of all confirmed binary systems, in particular distant but short periodic systems, show RUWE $\lesssim 1.4$ (Beck et al. 2024). RUWE, therefore, is an indicator for possible binarity but is not suited as an diagnostic to exclude a secondary companion. In their comprehensive catalog[3], Godoy-Rivera et al. (2025) have conducted a detailed search amending the binary indicators of *Gaia* by membership in binary catalogs from ground-based observations for *Kepler* targets, presented in the Binary Union Flag (BUF). Given the constructive nature of this catalog, this binary flag is dominated by RUWE as the primary indicator for binarity.

In total, we find 1296 binary candidates that are brighter than $G \leq 13$ mag. Table 1 provides the individual sample sizes. The position of stars from the APOKASC 3 and APO-K2 samples that are listed in the NSS are depicted in the first, second, and fourth panel of Fig. 1. Additionally, we added 49 binaries with oscillating MS or postMS primaries[4], found by Beck et al. (2024).

2.4. Rapid rotating red giants

Finally, we focus on the subsample of the rapid rotators in the APOKASC 3 sample. In a previous study, Patton et al. (2024) has identified ~1500 active red giant candidates from the full APOGEE DR16, whose projected rotation velocity exceeds $v \sin i \geq 5$ km/s. For the stars with asteroseismic solutions from *Kepler* observations, Pinsonneault et al. (2025) determined mass, radius, and the evolutionary state for 332 objects. We include this subsample, depicted in Fig. 2, as such enhanced rotation could be the signature of merger products or post-common envelope phases (Kochanek et al. 2014).

[3] The *Kepler-Gaia* catalog files are electronically available for download from https://zenodo.org/records/14774100.
[4] The *Kepler*/TESS-*Gaia* Binary catalog files are electronically available for download from CDS through the reference J/A+A/682/A7.

3. Evolution of binary fraction

Systems with orbital periods that are not sufficiently wide to allow the giant to expand freely until the tip of the RGB will undergo a common-envelope (CE) phase, likely leading to a short-lived destructive interaction. Consequently, the binary fraction is expected to decrease between the main sequence and the RGB and RC phases. However, the lack of consistent and complete binary indicators for large ensembles in the past made it difficult to estimate the evolutionary depletion of binary systems. From their large sample study of RV variations in APOGEE data, Badenes et al. (2018), reported a ~60% reduction from MS to RGB, with an estimated uncertainty of ~20%.

The determination of the binary fraction relies on the indication of stellar multiplicity rather than having the full set of orbital parameters for each system. Therefore, we use the Binary Union Flag from Godoy-Rivera et al. (2025), which offers the most comprehensive compilation of all available binary indicators for stars in the *Kepler* field of view. As such compilation of binary markers is not yet available for the APO-K2 sample, we only compute the binary fraction from the APOKASC 3 sample, as combining both samples would lead to a skewed result due to the differing completeness factors between the two catalogs.

The rich and homogeneous asteroseismic and spectroscopic dataset of the APOKASC 3 catalog provides an ideal opportunity to investigate the reduction of the binary fraction with advancing stellar evolution. We construct a magnitude-limited sample to determine a robust estimate of the binary fraction. The binary detection using *Gaia* shows an explicit cutoff with $G \lesssim 13$ mag (Gaia Collaboration et al. 2023a), which is brighter than the faint and well-populated end of the sample of oscillating red giants from the *Kepler* mission ($G \lesssim 15$ mag). We, therefore, adopt $G < 13$ mag as the faint and *Gaia*'s saturation limit of $G > 4$ mag as the bright cutoff of our sample. Table 1 reports the number of oscillating stars categorized by the seismically inferred evolutionary state of the asteroseismic primary.

3.1. Evolutionary subsample definition

Depending on its mass, a red-giant star can undergo two very distinct evolutionary channels (for details see the monographs by, e.g. Kippenhahn et al. 2013; Salaris & Cassisi 2005; Pinsonneault & Ryden 2023). The masses of giants in the APOKASC 3 catalog are dominated by low-mass stars but extend up to ~3 $M_\odot$ (Fig. 2). If the stellar mass is $M/M_\odot \lesssim 1.8$, the inert helium core degenerates fully before reaching the ignition temperature of He. As a result, the star must ascend the RGB and continue to expand while the core heats up. With the onset of quiescent He-core burning at the tip of the RGB ($R/R_\odot \simeq 200 \simeq 1$ AU), following a series of off-center helium flashes, the star settles into the RC phase (Bildsten et al. 2012). Stars more massive than this limit ($M/M_\odot > 1.8$) ignite their helium core before it degenerates, doing so at significantly smaller radii on the RGB ($200 \gtrsim R/R_\odot \gtrsim 80$), and subsequently settle into the 2RC.

Furthermore, we must consider the differing binary fractions of progenitors of the red-giant stars in the sample. On the main sequence, the binary fraction is a strong function of the mass of the primary component (Lada 2006). The main-sequence progenitors of these more massive stars are early to mid-A-type stars. While 40 - 50% of all solar-like dwarfs stars (G and mid F) are found to be in binary systems, this fraction increases to 50 - 70% for the more massive early F and A-type stars on the main sequence (e.g., Offner et al. 2023; Moe & Di Stefano 2017).

The precise seismically inferred masses allow for an effective separation between the degenerate and non-degenerate evolutionary channels in the red-giant phase to test for these population differences. We, therefore, evaluate the binary fraction separately for these two evolutionary regimes ($M \gtrless 1.8\,M_\odot$).

3.2. Binary fraction evolution for solar-like stars into the RC

Solar-like oscillating dwarfs constitute the progenitor sample for the giant stars that follow the evolutionary channel leading into degenerate He-core ignition. We, therefore, use the sample of 620 oscillating solar-like MS and subgiant (post-MS) stars observed by *Kepler* (Chaplin et al. 2011; Mathur et al. 2022) to estimate the main-sequence baseline binary fraction.

Using the Union Binary Flag from Godoy-Rivera et al. (2025), we identify 195 binary candidates in this sample, yielding a binary fraction of 31.5%. This value is in good agreement with the binary fraction of 35% reported by Badenes et al. (2018) for main-sequence stars in the sample of APOGEE, showing that for this sample the possible selection bias potentially introduced by basis the analysis on solar-like oscillating stars is small for the reference sample However, both values are well below the expected ~50%, suggested by large-sample statistics. For Badenes et al. (2018), this discrepancy can be explained by the nature of APOGEE spectroscopy, where some binaries remain undetected due to the suboptimal sampling of the observations or inclination effects. The binary indicators in the Union Binary Flag are dominated by *Gaia* RUWE measurements (accounting for 76.5% of binary candidate indicators). As mentioned before, ~40% of confirmed SB9 binaries have RUWE ≤ 1.4 (Beck et al. 2024), which suggests that a significant fraction of binaries in our sample might remain undetected due to weak photocentric motion.

For the computation of the binary rate on the main sequence, we should consider that this sample could be biased against binarity. From the sample of Mathur et al. (2022) we find that about 50% of all dwarfs observed by *Kepler* show solar-like oscillations. Mathur et al. (2019) argued that the non-detection of mode is probably caused by high levels of activity, low metallicity, or tidal interaction, which reduce the oscillation amplitudes below the detection limit. The latter assumption was motivated from the finding that red-giant in binary systems show suppressed oscillation, once the fractional radius of both components fills more than ~20% of the semi-major axis a, i.e. $(R_1 + R_2)/a \gtrsim 20\%$, and the tidal spin up activates a stellar dynamo (Gaulme et al. 2014). Such fractional radius coincides with the threshold of tidal interaction through the equilibrium tide for the circularization and synchronization (Beck et al. 2018b). However, Beck et al. (2024) showed that solar-like stars in strongly interacting binary systems that are synchronized and circularized by the dynamical tide ($P_{\rm orb} \lesssim 8$ days, Zahn 1989; Raghavan et al. 2010) can exhibit solar-like oscillations even at high levels of photospheric activity. Among the 663 non-oscillating MS and post-MS, we find 270 binary candidates from the binary union flag, which corresponds to a binary fraction of ~40.7%, which suggests that binarity might have a small effect but is not the dominant mechanism to reduce the amplitude of solar-like oscillations in MS stars. Therefore, we consider this base value provides a good reference for the binary fraction on the main sequence.

From comparing the numbers, we argue that our survey, as reported in this paper, has a completeness factor between 60 and 80%. In this paper we report the binary fractions uncorrected for the completeness factor. We assume this completeness factor is constant throughout the subsequent evolutionary states.

Table 1. Binary fraction in the sub-phases of the red-giant star evolution.

Evolutionary state	Full Sample Stars	Mag. Limited ($M/M_\odot \leq 1.8$) Stars	Bin.Sys.	Bin.Frac.	Mag. Limited ($M/M_\odot > 1.8$) Stars	Bin.Sys.	Bin.Frac.
MS & post-MS (oscillation detected)	620	620	195	31.5 %	–	–	–
MS & post-MS (no oscillation)	663	663	270	40.7 %	–	–	–
H-shell burning / RGB	7191	5331	438	8.2 %	447	43	9.6 %
low-luminosity RGB	4103	3209	310	9.7 %	139	18	12.9 %
high-luminosity RGB	3088	2122	128	6.0 %	308	25	8.1 %
He-core buring (RC & 2RC)	5560	3881	200	5.2 %	982	134	13.6 %

Notes. The left panel specifies the evolutionary states and gives the number of all stars with this identified phase in the catalog. The red-giant stars are based on APOKASC 3 (Pinsonneault et al. 2025), while the main-sequence dwarfs and subgiants are taken from the sample of Mathur et al. (2022). For the RGB, we first provide the full range and then separate between the case of the low- ($\nu_{max} \geq 30\,\mu$Hz) and high-luminosity regime ($\nu_{max} < 30\,\mu$Hz). The center and right panel separate the stars by their mass regimes leading to the degenerated ($M/M_\odot \leq 1.8$) and non-degenerated ($M/M_\odot > 1.8$) ignition of the He core, respectively. Both panels' first, second, and third columns indicate the number of stars, binaries identified through the Binary Union Flag (Godoy-Rivera et al. 2025), and the corresponding binary fraction in percent for the respective evolutionary state.

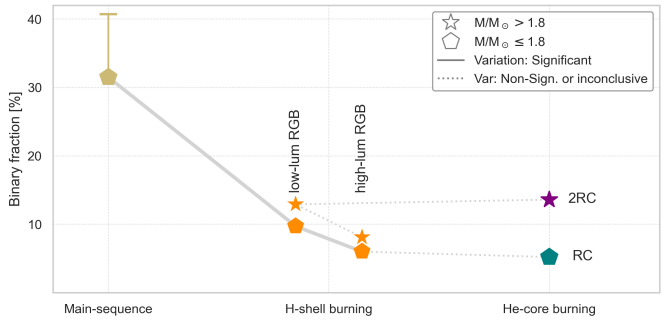

Fig. 4. Binary fraction as a function of their evolutionary states. Pentagons mark stars that undergo core-degeneration on the RGB ($M/M_\odot \leq 1.8$), while star symbols indicate the binary fraction for stars that will ignite He under non-degenerate conditions ($M/M_\odot > 1.8$). The style of the connecting lines depicts the significance of the variations as discussed in the text and specified in Table 2. The yellow bar indicates the binary fraction among MS stars without oscillations. The marker color depicts the evolutionary state as indicated on the horizontal axis.

For stars with masses below 1.8 $M_\odot$, we find 438 binary candidates with RGB primaries and 200 with primaries in the RC, corresponding to binary fractions of 8.2% for the H-shell and 5.2% for the He-core burning stars that exhibit solar-like oscillations (Table 4 and Fig. 1). From these numbers, we estimate a binary attrition from the main sequence to the RGB phase to be ~69% (Table 2), which is in good agreement with the reduction found in the APOGEE sample (Badenes et al. 2018). The binary depletion is even larger between the main-sequence and the red-clump phase with ~84%.

With a maximum change of the stellar radius of nearly two orders of magnitude, the RGB is the phase with the most significant variations and differences in stellar radius. Therefore, a significant reduction along the RGB evolution itself can be expected. To test this variation, we use the peak frequency of the oscillation power excess, ν_{max}, to divide the RGB into two subsamples and evaluate their binary fraction separately. For the low-luminosity RGB ($300 \gtrsim \nu_{max} \geq 30\,\mu$Hz, which correspond to approximately to a range in radius of $3 \lesssim R/R_\odot \lesssim 10$) we find a binary fraction of 9.7%. For the high-luminosity RGB ($30 > \nu_{max} \gtrsim 0.1\,\mu$Hz, $10 \lesssim R/R_\odot \lesssim 100$) we find a binary fraction of 6.0%. This corresponds to an attrition of ~38% from the low- to the high-luminosity RGB, of ~81% with respect to the MS. For the detailed overview of the values, we refer the reader to Fig. 4, as well as Tables 1 and 2.

Table 2. Binary attrition between evolutionary states and samples.

Track or comparison	Rel. Decrease	p
MS → low-lum. RGB	69.3 %	10^{-40} (h)
MS → high-lum. RGB	80.8 %	10^{-66} (h)
MS → RC	83.6 %	10^{-102} (h)
low-lum. RGB → high-lum. RGB	37.6 %	10^{-6} (h)
low-lum. RGB → RC	46.7 %	10^{-13} (h)
high-lum. RGB → RC	14.6 %	0.15 (n)
low-lum. RGB → high-lum. RGB	–	0.12 (n)
high-lum. RGB → 2RC	–	0.93 (n)
osc. MS ⇔ non-osc MS	29.2 %	10^{-4} (h)
deg RGB ⇔ non-deg RGB	17.1 %	0.01 (m)

Notes. The table reports the significance levels of the binary attrition depicted in Fig. 4. The first column indicates the evolutionary states that are compared. The second column indicates the relative decrease of the binary fraction in percent. The final column indicates the variation's significance from a χ^2 test, as described in the text. The table's top and middle panels represent the tracks that undergo He-core ignition under degenerated and non-degenerated conditions. The bottom panel compares the average binary fraction between the indicated samples.

We applied the χ^2 test for independence to evaluate whether the observed differences in binary fractions between evolutionary states are statistically significant, under the null hypothesis that binarity is independent of stellar evolutionary phase. We adopt the traditional threshold-based classification of p-values, whereby results with $p < 0.001$ are deemed highly significant, indicating strong statistical evidence against the null hypothesis. When p-values fall in the range $0.001 \leq p < 0.05$, the variation is deemed marginally significant, suggesting a moderate likelihood that the observed difference is not purely due to statistical fluctuations. Conversely, if $p \geq 0.05$, we classify the variation as insignificant. The significance test, whose results are reported in Table 2 and depicted in Fig. 4, shows that the binary attrition from the main sequence to any state of the giant branch and the RGB to the RC are significant. It is worth highlighting that the ~38% reduction between the low- and high-luminosity regime of the RGB evolution is highly significant. The only variation not found to be significant in the low-mass sample is the reduction of ~15% from the high-luminosity RGB into the RC phase. To determine whether the small variation between the high-luminosity RGB and the RC is real, a larger sample would be required.

Finally, we note that two important potential biases exist for this analysis. First, the selection criterion on solar-like oscillations introduces a bias. As mentioned before, it was shown that solar-like oscillations are suppressed in giants where the combined fractional stellar radii exceed ~20% of the system's semi-major axis. Consequently, stars starting to fill their Roche-lobe substantially will also be excluded from the sample of oscillating giants. However, once this phase has started, the time scales of a few 100 kiloyears, leading into a potentially destructive evolution and white-dwarf phase, are short. Given the duration of the RGB phase, this dilution effect does not skew the sample significantly. Second, stellar oscillations are also detectable from RV variations. However, only on the super-luminous RGB ($\nu_{\rm max} \lesssim 0.1\,\mu$Hz, or $100 \lesssim {\rm R/R_\odot} \lesssim 200$), the RV amplitude of stellar oscillations becomes substantial enough to reach or exceed the RV threshold of ~1.4 km/s (Katz et al. 2019) for faint stars of the *Gaia* RVS instrument ($G \lesssim 12$ mag). As this regime is not probed by the frequency range of the APOKASC 3 catalog, possible false positive binary solutions produced by intrinsic stellar RV variations do not bias this comparison.

3.3. Evolution of the binary fraction for 2RC giants

The progenitors of secondary clump stars are early F- and A-type stars, which exhibit a different type of pulsations (γ Dor and δ Scuti, Aerts et al. 2010, and references therein). Therefore, these are not represented in the main-sequence sample of Mathur et al. (2022). We measure the binary fraction for the non-degenerate evolution starting from the low-luminosity RGB.

Table 1 and Fig. 2 show that such relatively massive stars represent only a small fraction of the full APOKASC 3 sample. Consequently, their population and binary counts suffer from small-number statistics, and all variations found between the subsamples were determined to be non-significant. The only marginally significant difference that we found from the numbers in Table 2 was that the binary fraction of the full sample of non-degenerate RGB stars (~9.6%) is ~17% richer in binaries than the full sample of degenerated RGB (~8.2%). This difference agrees with the differences in the binary fraction of their main-sequence progenitors, known from large binary statistics.

4. Co-evolution of the primary mass and the orbit

The key parameter determining the evolution of a star is its initial mass (Serenelli et al. 2021, and references therein). It defines the stellar structure and timescales of the evolution. In a binary system, the total mass of the components, together with the semimajor axis a or orbital period $P_{\rm orb}$, defines the system's configuration through the third law of Kepler (1619),

$$\frac{a^3}{P_{\rm orb}^2} = M_1 + M_2. \quad (1)$$

Thus, stellar mass dictates the evolution of individual stars and influences the properties and evolution of binary and planetary systems through tidal interactions and mass loss.

Tidal interactions gain importance when the radius of one of the stellar components grows to a significant fraction of the semimajor axis. The redistribution of angular momentum and dissipation of kinetic and potential energy from tides into heat drives the changes of the orbits and the spins. This process leads the system toward a state of minimum energy, where the orbit is circularized, and the stellar spins become aligned and synchronized (Zahn 1977; Ogilvie & Lin 2007; Mathis 2015). Tidal interaction occurs in waves as dynamical tide or hydrostatic adjustment in the equilibrium tide, whereby the stellar structure, which depends primarily on the stellar mass, determines the dominant tidal mechanism. The various manifestations of tides are intensively studied from the distributions of the orbital parameters in large samples from open clusters or the *Gaia* mission, providing valuable constraints on tidal dissipation and orbital evolution (e.g. Mirouh et al. 2023; Dewberry & Wu 2025).

Mass loss during stellar evolution, such as stellar winds, also affects orbital evolution by removing mass and angular momentum from the system (Miglio et al. 2012). Following Kepler's third law (Eq. 1), this leads to an increase of the orbital period (Zahn & Bouchet 1989; Soberman et al. 1997) and also to the spin-down of the mass-loosing star (e.g. Skumanich 1972).

The evolution of a binary system becomes particularly complex once one component fills its Roche lobe and significant mass transfer occurs. This process can either shrink or widen the orbital separation, depending on the mass ratio and angular momentum exchange (Ivanova et al. 2013, and references therein). At the same time, the donor star's radius is increasing. Red giants, which possess convective envelopes, expand in response to mass loss in order to preserve an approximately constant entropy profile (Hjellming & Webbink 1987). Moreover, tidal heating in close systems may further inject energy into the stellar envelope, contributing to additional expansion (Gallet et al. 2017). This expansion, occurring on timescales much shorter than the evolutionary pace can destabilize mass transfer in close binaries, leading to runaway expansion of the donor.

If the radius of one of the binary components exceeds the orbit of the companion, the system will enter the short-lived, most likely destructive common-envelope (CE) phase, which would end the red-giant phase of the star abruptly with the CE ejection, exposing the "naked" He-core as a white dwarf (Ivanova et al. 2013). Due to the hydrodynamical complexity and their short time scales, this phase is difficult to model and poorly understood (Han et al. 2002). However, several parameters are identified to play a significant role in determining the fate of the binary system. The primary determining factor is the semimajor axis relative to the maximum stellar radius of the components, as this governs both tidal interaction strength and the Roche-lobe radius. Furthermore, the mass ratio between the two stars, which influences the difference in their evolutionary timescales (e.g. Miglio et al. 2014; Beck et al. 2018a; Grossmann et al. 2025)

Another critical parameter is if the mass loss is stable or unstable (Podsiadlowski 2001). It is important to note that the mass loss rate of the donor is substantially larger than the accretion rate of the accretor. In case of stable mass loss, the mass ratio q will be gradually adjusted, allowing the system to adapt continuously by expanding its orbit and shifting to longer orbital periods. Such a system will not undergo a common envelope or merger phase. In the case of non-stable mass loss, the orbit is shrinking, leading to a CE phase. It is still unclear what determines the fate of a binary system at the end of the CE phase. If a system enters a CE phase, envelope ejection depends on whether the orbital energy released during the spiral-in phase exceeds the envelope's binding energy. Generally, systems with extreme mass ratios ($q = M_2/M_1 \ll 1$) are unlikely to inject sufficient orbital energy to expel the envelope, leading to a merger event (Ivanova et al. 2013).

Since stellar ages are typically inferred from model fitting, based on single-star evolutionary models assuming steady mass loss (e.g. Pinsonneault et al. 2025), episodic or interaction-induced mass loss in binary systems will significantly over- or underestimate the ages of the post-interaction stellar products.

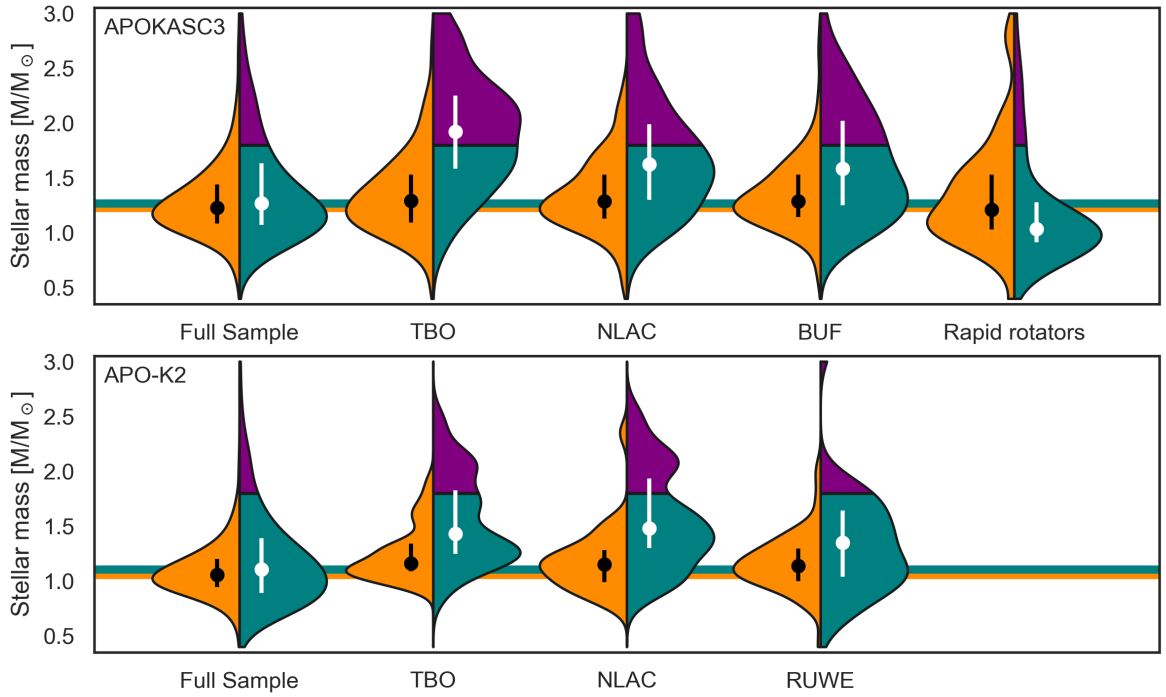

Fig. 5. Normalized kernel density estimates of the stellar mass distributions for red giant stars in the APOKASC 3 (top) and APO-K2 (bottom) samples. Each KDE is split by evolutionary stage, with the left side (orange) showing RGB stars and the right side displaying core-helium burning stars. The latter are further divided into RC (teal) and 2RC (purple) stars, separated at 1.8 $M_\odot$. Distributions are shown for the full sample and several binary candidate subsamples identified by the TBO, NLAC, and Binary Union Flag (BUF) for APOKASC 3 and RUWE for APO-K2, as well as the rapid rotator subset in APOKASC 3. Dots and vertical bars indicate the median and interquartile range (25^{th}–75^{th} percentiles) for each population. Horizontal orange and teal lines mark the median RGB and RC stellar masses of the respective full samples.

4.1. Mass distributions separated by evolutionary state

To isolate evolutionary effects in the binary sample, we construct reference mass distributions for the entire sample, separated by evolutionary state. Since the mass distributions differ between the APOKASC 3 and APO-K2 catalogs, we analyze these two catalogs separately to avoid potential systematic biases in the samples skewing the result. The resulting KDE, shown in Fig. 5, show that the mass distribution among in the full samples are similar. Furthermore, Fig. 5 presents KDEs for the mass distributions for samples selected from various binary indicators. In the RGB phase, the mass distribution of all binary markers closely resembles that of the full sample, with only minor deviations.

A very different picture emerges when examining the binary sample of stars RC and 2RC stars. The mass distribution of stars that have that have ignited their He-core is significantly shifted Fig. 5. While the full sample of He-core burning stars in the APOKASC 3 sample has a median mass of 1.27 $M_\odot$ and the interquartile range (25^{th}–75^{th} percentiles) between 1.07 and 1.63 $M_\odot$, the median mass for RC and 2RC stars in binary systems with orbital periods from the TBO is 1.92 $M_\odot$ and their interquartile range between 1.58 and 2.25 $M_\odot$. A similar trend is found for binary stars hosting He-core burning stars from the APO-K2 ample and TBO orbital solutions (Fig. 5).

Figure 5 presents similar shifts in the mass distributions of He-core burning stars from samples identified through different binary indicators. The most pronounced difference is observed for binaries identified in the *Gaia* TBO catalog. The comparison with the SB9 catalog by Beck et al. (2024) suggests that it predominantly contains orbits with resolved periods of $P \lesssim 1500$ days, while NLAC solutions typically indicate longer-period systems. We argue that the *Gaia* TBO catalog is more sensitive to the depletion of short-period systems. Since the Binary Union Flag indicator depends largely on RUWE, they are also sensitive to long-period binaries. This trend is consistently observed in both the APOKASC 3 and APO-K2 catalogs, excluding that this results from a selection bias.

We suggest that these differences in mass distributions arise from disruptive and merging events along the RGB as shorter periodic systems undergo a CE phase, mostly leading to the deconstruction of the giant in the binary system. This process introduces a stronger mass dependence on the binary fraction than for the main sequence progenitors. As the main parameter to determine if a system will undergo the CE phase is the period, we expect a mass-period relation in the He-core burning phase.

4.2. Mass dependency of the orbital parameters

For intermediate periods ($8 \lesssim P_{orb}\,[d] \lesssim 10^4$), orbital eccentricities e of MS binaries follow a Maxwellian "thermal" distribution (Zahn 1989; Raghavan et al. 2010; Moe & Di Stefano 2017), indicating that the probability density increases linearly with e, i.e., systems with higher eccentricities are more common than low or circularized eccentricities which is still present in the eccentricities of main-sequence stars in Fig. 6.

The combined large sample of binary stars with orbital solutions from the TBO with seismically inferred evolutionary states and masses from the APOKASC 3 and APO-K2 allows us to populate the eccentricity-period (e-P) plane (Fig. 6) and study the binary evolution as a function of stellar evolution (Fig. 7). We find a significant reduction in the ranges of orbital period and eccentricity from the main sequence into the He-core-burning phase. The short-periodic end of the period distribution is mov-

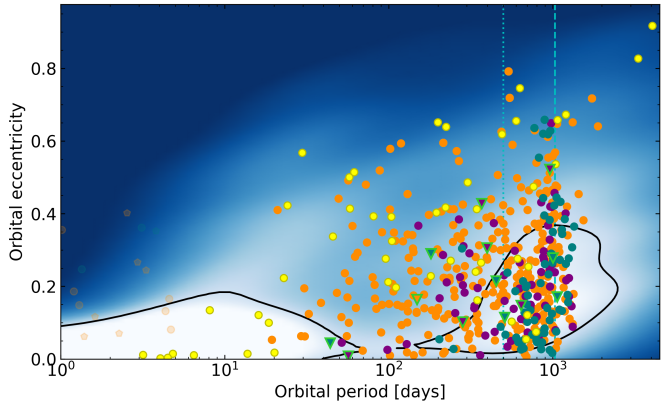

Fig. 6. Orbital parameters of binary systems with seismically inferred evolutionary states. In addition to the color code for the evolutionary states of red giants (Fig. 1), oscillating MS+postMS primaries are shown in yellow. Stars found to be rapid rotators are marked as triangles. The background color map represents the KDE of the full SB9 catalog, with black lines outlining regions where the density exceeds seven times the median value. Vertical dashed and dotted lines represent the 1034 d timebase of *Gaia* DR3 and ~500 d limit for RGB stars with degenerate cores to evolve as single stars. Likely artifact solutions for giants ($P_{orb,TBO} \leq 10$ days) are shown with a lower opacity.

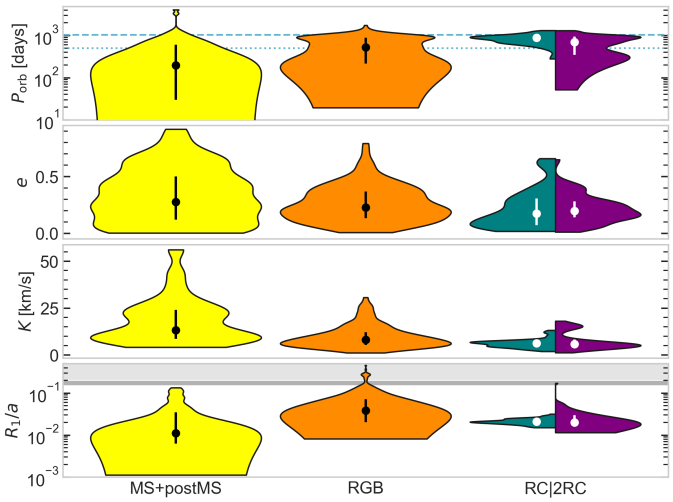

Fig. 7. KDEs of orbital parameters (e, P), the RV semi-amplitude K, and fractional radius R_1/a for the binary population identified by the *Gaia* TBO for solar-like oscillators. The distributions are grouped by evolutionary stage, with the rightmost violin in each panel split to show red clump (RC, teal) and secondary clump (2RC, purple) stars. Dots and vertical bars indicate the median and interquartile range (25^{th}–75^{th} percentiles) of each group. Horizontal dashed and dotted lines in the top panel mark the *Gaia* DR3 time baseline (1034 d) and the ~500 d upper limit for binary interaction during the RGB phase for stars with degenerate helium cores. The shaded grey region in the bottom panel marks the regime of strong tidal interaction ($R_1/a > 15\%$).

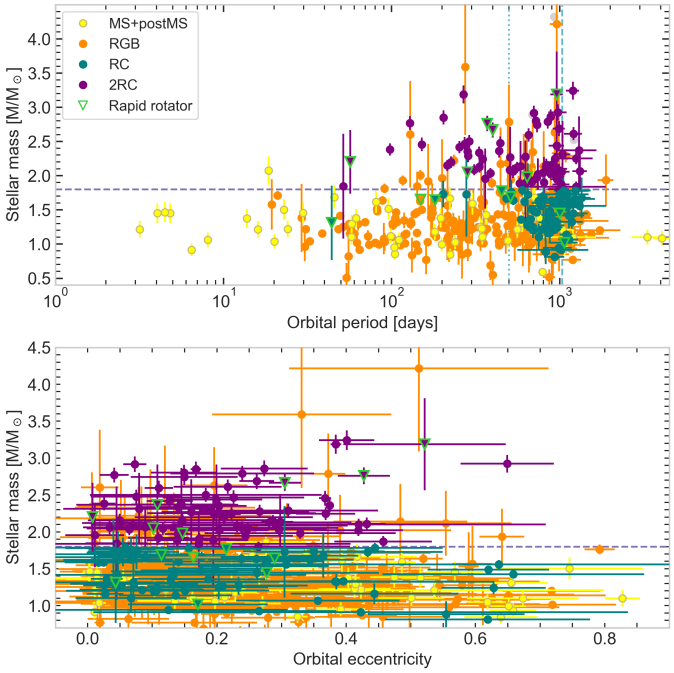

Fig. 8. Orbital period and eccentricity as a function of the primary's mass. Colors, symbols, and the vertical dashed lines have identical meanings, as described in the caption of Fig. 6. The horizontal purple line marks the chosen separating mass between RC and 2RC.

ing from a few days for mains-sequence stars to about 20 days for RGB. For stars in the He-core burning phase, the short periodic end is 200 and 500 days for 2RC and RC stars.

We further inspected the correlation between mass and orbital period as a function of the evolutionary state (Fig. 8). For MS and RGB stars, we find the masses mostly uncorrelated with the periods. However, for He-core burning stars, a clear inverse correlation is found between the primary mass and the orbital period of a system. In particular, hardly any system with a primary mass $M \leq 1.8\,M_\odot$ is found on orbital periods below 500 days. This supports the assumption that this difference in the cut-off periods results from the lower maximum radius at the tip of the RGBs for stars with $M > 1.8\ M_\odot$, allowing stars in smaller systems to complete the RGB phase without significant interactions.

Systems hosting helium-core burning stars show interesting dependencies of the eccentricity with their orbital period. Figure 6 reveals that the sample of RC stars with $P_{orb} \gtrsim 800$ days have a wide spread in eccentricity similar to the stars ($e \lesssim 0.7$), while for systems with $500 \lesssim P_{orb} \lesssim 800$ days the eccentricity is $e \lesssim 0.25$. This step in the eccentricity distribution could suggest an increased strength of tidal interactions up to this limiting period for systems hosting RC stars. The wider eccentricity range for the more massive 2RC stars ($e \lesssim 0.4$) is explainable with the smaller radius and weaker tidal interaction at their He-core ignition. However, the steep increase and over-density of RC, 2RC, and RGB systems around 1,000 days could also be partially an artifact. The comparison of *Gaia* TBO with SB9 by Beck et al. (2024, see Fig. 2 and A.1) showed that systems longer than the DR3 baseline of 1034 days have periods around 1,000 days. The increased baseline from *Gaia* DR4, which is twice that of DR3, will help to test if this is an instrumental artifact.

4.3. Post-common envelope systems

We find numerous short periodic systems among the systems shown in the e-P plane in Fig. 6. Such systems are most likely artifacts of longer-periodic systems in the TBO. While red giants could exist in short-period systems, it is unlikely that such primaries would exhibit solar-like oscillations due to the effects of tidal interactions. We, therefore, excluded systems with $P_{orb,TBO} \leq 10$ days from the analysis but show them in Fig. 6.

Figures 6 and 8 present several binary candidates from *Gaia* TBO, which are hosting a He-core burning RC star at orbits significantly smaller than 500 days. If such systems are real, these would be post-CE binary systems. When the secondary component does not spiral down deep enough to reach the bottom of the

convective envelope, it is also possible that it survives in the convective envelope on an orbit smaller than the maximum radius of the giant at the tip of the RGB (Ivanova et al. 2013). It is striking that most RC primaries of these systems also have rotationally broadened absorption lines in APOGEE spectroscopy (triangle markers). Such an enhanced surface rotation could indicate a spin-up of the primary envelope during the CE phase, which had further spun up during the contraction when the star was settling into the RC after helium ignition. Our ongoing spectroscopic follow-up observations will testing if the orbital parameters from in the TBO for those particular systems are correct.

While the mass distribution of rapidly rotating giants in H-shell burning RGB phase also follows the distribution of the entire sample (median: 1.21 $M_\odot$, interquartile range: 1.03 to 1.53 $M_\odot$), it strongly deviates in the He-core burning phase (median: 1.03 $M_\odot$, interquartile range: 0.91 to 1.28 $M_\odot$, Fig. 5). Such difference supports the assumption that these stars have undergone a disruptive phase and lost larger fractions of their mass than would be accounted for from steady wind-driven mass loss, rendering ages from single star models unreliable.

Only ~7.5% of all giants with enhanced surface rotation are found to be in binary systems. Although this is slightly above the overall binary rate for RC stars, this is notable, as Patton et al. (2024) reported from all available binary indicators from *Gaia* DR3 and APOGEE RVs, a binary fraction of 73±2% for the entire sample of giants with enhanced surface rotation. This is significantly higher than the expected binary fraction of low-mass stars on the main-sequence, which indicates that these are the products of merger and disruptive events.

5. Evolution of the radial velocities

The accumulated combined effect of stellar evolution and tidal interactions are propagating into the most commonly observed property of a binary system, the RV semi-amplitude,

$$K_{1,2} = \frac{M_{2,1}}{M_1 + M_2} \frac{(2\pi G)^{1/3}}{P_{\rm orb}^{1/3}} \frac{\sin i}{\sqrt{1-e^2}}, \quad (2)$$

with i being the inclination of the orbital plane. From classical mass loss and the tidally driven circularization of the orbit, a decrease in the RV amplitude is expected with continued age.

From the evolution of K with respect to $\log g$, Badenes et al. (2018, Fig. 5) reported a significant attrition of the peak-to-peak amplitude from ~200 km/s on the MS to ~30 km/s at the RGB tip. To test if we find a similar accumulated effect in the seismically characterized APOKASC 3 and APO-K2 samples, we use K provided in the TBO (Gaia Collaboration et al. 2023a).

5.1. RV vs orbital period and stellar radius

Figure 9 (top panel, see also Fig. 7) depicts an apparent reduction of the semi-RV amplitude from the MS is where semi-amplitudes of nearly 100 km/s are found. On the low-luminous RGB, K $\lesssim$ 30 km/s are found, but are reduced to K $\lesssim$ 20 km/s on the luminous RGB. Most RC and 2RC systems are found with K $\lesssim$ 10 km/s, with a few systems reaching $K \lesssim 20$ km/s.

When comparing these numbers with Badenes et al. (2018), we need to take into account that they are using the peak-to-peak variation, which is up to twice the semi-amplitude K. Therefore, the values presented in Fig. 9 are in good agreement with large-sample spectroscopic studies. The detection threshold value for a significant RV variation with the *Gaia* RVS instrument is 0.3 and 1.4 km/s for bright and faint stars (Katz et al. 2023). Given

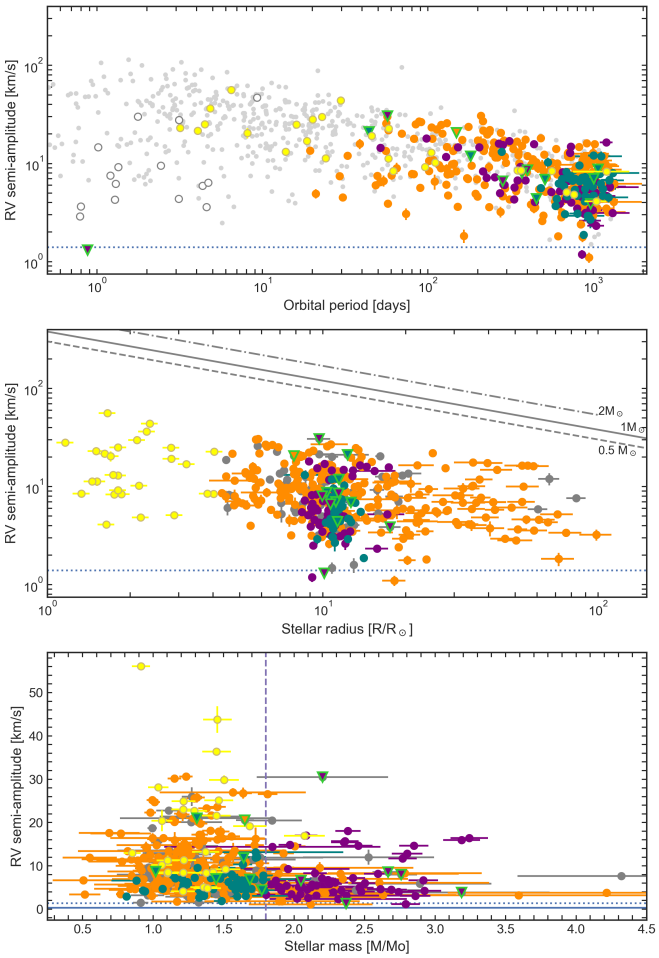

Fig. 9. Evolution of the radial velocity semiamplitude of the binary motion as a function of the orbital period (top), stellar radius of the primary from *Gaia* parameters (middle), and the seismically inferred mass (bottom panel). The colors of the dots represent the various evolutionary states and are identical to Fig. 1, and 6. The dotted and solid horizontal lines in the top and bottom panel depict the detection threshold of the RVS instrument for faint and bright stars, respectively. The grey lines in the middle panel depict the radial velocities for binary systems whose Roche lobe radius is filled. In the bottom panel, the vertical purple line marks the chosen separation between RC and 2RCstars.

the typical K in red-giant binary systems and brightness of targets of *Kepler* space photometry, this value RV floor is sufficient. Similarly, a reduction of K is also seen as a function of the stellar radius (Fig. 9). Figure 7 shows that we find a cutoff of the oscillating sample of RGB stars at a fractional radius of $R_1/a \gtrsim 20\%$. We further note that MS+postMS and the core-He burning (RC+2RC) stars are well below this threshold (Fig. 7).

The reduction of K for RC and 2RC systems can be interpreted as a combined consequence of orbital circularization on the RGB, when the expanded envelope leads to large fractional radii and strong tides, and the effect of wind-driven mass loss, enhanced by the extreme stellar luminosities near the RGB tip.

To test if red-giant primaries are close to filling their Roche lobes, we estimated the critical period, $P_{\rm RL}$. We follow the formalism of Eggleton (1983),

$$P_{\rm RL} = 2\pi \cdot \mathcal{R}(q) \cdot \sqrt{\frac{R^3}{GM}}, \quad (3)$$

where $\mathcal{R}(q)$ is the ratio between the radius of the Roche Lobe and the orbital separation, and q is for the mass ratio, which we

assume to be at unity. Following Eggleton (1983), $\mathcal{R}(q = 1)$ can be approximated by 0.38. The resulting velocities for 0.5, 1, and 2 $M_\odot$ filling their Roche lobe are depicted as grey lines in Fig. 9. The gap between the detected systems and the Roche-lobe limit can be attributed to the suppression of modes due to enhanced activity driven by the increasing strength of the equilibrium tide. Therefore, those systems are far from filling their Roche lobe.

5.2. RV vs stellar mass

For He-core burning stars, no specific trend is found with mass, except for a few outliers ($K \lesssim 20$ km/s), in particular among the 2RC. An interesting trend is found for the RGB stars, where the range for stars with $M \leq 1.8\,M_\odot$ reaches up to 30 km/s, while for systems with a more massive primary, we find a similar range of RVs as for helium core burning stars. The RGB stars with the large K are typically in shorter-periodic binaries ($P_{orb} >\lesssim 300$ days) which leads to higher K values (Eq. 2).

6. Discussions and conclusions

In this paper, we investigated the binary properties of red-giant stars by combining asteroseismic constraints from the APOKASC 3 and APO-K2 catalogs with binary solutions from *Gaia* DR3's NSS catalog. The asteroseismically inferred stellar masses and evolutionary states provide key diagnostics for characterizing binary systems hosting solar-like oscillators. This cross-matched dataset enabled a comprehensive analysis of how binary fraction, stellar mass distribution, and orbital parameters evolve across different evolutionary stages, offering a holistic view of stellar–binary co-evolution.

Our results demonstrate a significant reduction of the binary fraction as stars ascend the RGB and transition into the core-helium burning phase. To account for distinct evolutionary pathways, we divided the sample based on asteroseismic masses into low-mass stars ($M \leq 1.8\,M_\odot$), which develop fully degenerate helium cores, and intermediate-mass stars ($M > 1.8\,M_\odot$), which ignite helium under non-degenerate conditions. We find that approximately ~31.5% and ~40.7% of solar-like stars on the main sequence, that with detected and non-detected solar-like oscillations, respectively, are members of binary systems. This is a noteworthy result, as magnetic activity, often enhanced in close binaries, has been suggested to reduce solar-like oscillations in dwarfs. Using ν_{max} as a proxy for stellar luminosity, we further subdivided the RGB into low- and high-luminosity regimes. Our analysis reveals a significant reduction of ~69% in the binary fraction from the main sequence to the low-luminosity RGB, followed by a further ~38% decrease from the low- to high-luminosity RGB. Interestingly, no significant change in the binary fraction is found between the high-luminosity RGB and RC, suggesting that most binary attrition or interaction occurs earlier during the RGB ascent. For the intermediate-mass stars ($M > 1.8\,M_\odot$), we find a substantially higher binary fraction. This is consistent with the intrinsically higher binary occurrence rate (approx. 8 to 14%), observed among early F- and A-type stars on the main sequence. However, due to the smaller sample size in this mass regime, we are currently unable to robustly test for evolutionary changes in binary fractions across the MS.

From the comparison of the mass of binaries hosting RGB and RC and 2RC, we find that the mass distribution for He-core burning stars is significantly shifted to more massive stars. This suggests that mass transfer, envelope stripping, or merger events have shaped a significant portion of the population and introduced a mass-dependent bias in binary attrition.

The distribution of orbital parameters reveals a clear evolutionary trend. While main-sequence stars span a wide range of orbital periods, resembling the expected initial distribution, systems hosting RGB and core-helium-burning stars are predominantly found at longer periods and with reduced eccentricities. RC stars are typically found in systems with orbital periods longer than 500 days. In contrast, more massive 2RC are found at shorter periods, down to ~200 days. This reduction is interpreted as evidence of binary interaction or disruption, and is consistent with the fact that intermediate-mass stars ignite He with smaller radii on the RGB, allowing tighter systems to avoid interaction.

A few RC systems are detected with orbital periods shorter than 500 days, several of which exhibit signs of rapid surface rotation. These may represent candidates for post-CE systems or merger remnants resulting from previous mass transfer episodes. Such systems exemplify the rich variety of products associated with binary interaction and mass transfer, such as hot subdwarf B stars (sdB Vos et al. 2020), He-rich white dwarfs (Kilic et al. 2025), binarity among central stars of planetary nebulae (Jones & Boffin 2017), symbiotic systems (e.g., Merc et al. 2024), where an evolved giant transfers material to a compact companion, and chemically peculiar barium stars (e.g., Escorza et al. 2020). From the reduction of the RV semi amplitudes, we also show the accumulated effect of tidal interaction and mass loss.

As orbital periods approach ~800 to 1,000 days, corresponding to semi-major axes comparable to red giant radii, binary co-evolution becomes increasingly complex. In this regime, the otherwise simplifying assumption of co-evolution of both stellar components and the binary orbit is challenged. In particular, age estimates from single-star models may no longer be reliable for post-interaction products.

Our results provide clear observational evidence for mass- and evolution-dependent attrition of binary systems during the red-giant phase. These findings have important implications for binary population synthesis and the interpretation of chemical and rotational anomalies in evolved stars. In particular, the ages of helium-core burning stars may be misleading if prior mass loss or transfer is unaccounted for. Red-clump systems that have undergone substantial interaction are therefore unsuitable for calibrating stellar evolution models based on single-star physics. This study underscores the powerful synergy between asteroseismology and *Gaia* in unraveling stellar and orbital co-evolution, by providing valuable insights for more refined binary population synthesis and age-dating techniques.

The available samples of oscillating red giants in binaries are expected to grow substantially with upcoming data releases and forthcoming space missions. The extended time baseline and epoch spectroscopy provided by *Gaia* DR4 will significantly improve the census and precision of astrometric and spectroscopic binary solutions, particularly for long-period systems. The Science Calibration and Validation Plato Input Catalog (scvPIC) of ESA's PLATO mission (PLAnetary Transits and Oscillations of stars; Rauer et al. 2014, 2024) will further increase the number of oscillating stars in eclipsing and astrometric binary systems identified by *Gaia*. Additional contributions will come from NASA's Roman Space Telescope (Huber et al. 2023) and the Chinese Earth 2.0 mission (Ge et al. 2022), which will extend the ensemble of solar-like oscillators across diverse regions of the Milky Way. Together, these missions will provide the necessary data to probe binary evolution in the context of galactic archaeology. This underscores the need for a holistic picture of stellar and binary co-evolution. This is essential for accurately determining stellar ages and unlocking the full potential of red giants as tracers of Galactic history.

Acknowledgements. The author thanks the referee for useful comments that allowed us to improve the article. The author thanks the people behind the ESA *Gaia*, NASA *Kepler*, and NASA TESS missions and the APOGEE project. PGB thanks Santi Cassisi, Thomas Masseron, Joel Zinn, Savita Mathur, Diego Godoy Rivera, and Jaroslav Merc, for fruitful discussions on the catalogs and the paper manuscript. PGB acknowledges support by the Spanish Ministry of Science and Innovation with the *Ramón y Cajal* fellowship number RYC-2021-033137-I and the number MRR4032204, as well as the proyecto plan nacional *PLAtoSOnG* (grant no. PID2023-146453NB-100, PI: Beck). This research was supported by the International Space Science Institute (ISSI) in Bern, through ISSI International Team project 24-629 (*Multi-scale variability in solar and stellar magnetic cycles*).

This work has made use of data from the European Space Agency (ESA) mission *Gaia* (`https://www.cosmos.esa.int/gaia`), processed by the *Gaia* Data Processing and Analysis Consortium (DPAC, `https://www.cosmos.esa.int/web/gaia/dpac/consortium`). Funding for the DPAC has been provided by national institutions, in particular the institutions participating in the *Gaia* Multilateral Agreement. This paper includes data collected with the *Kepler* & TESS missions, obtained from the MAST data archive at the Space Telescope Science Institute (STScI). Funding for these missions is provided by the NASA Science Mission Directorate and by the NASA Explorer Program respectively. STScI is operated by the Association of Universities for Research in Astronomy, Inc., under NASA contract NAS 5–26555.

Software: `Python` (Van Rossum & Drake 2009), `numpy` (Oliphant 2006; Harris et al. 2020), `matplotlib` (Hunter 2007), `scipy` (Virtanen et al. 2020), `Astroquery` (Ginsburg et al. 2019). This research made use of `Astropy` (Astropy Collab. et al. 2013, 2018), a community-developed core Python package.

References

Aerts, C., Christensen-Dalsgaard, J., & Kurtz, D. W. 2010, Asteroseismology
Anders, F., Gispert, P., Ratcliffe, B., et al. 2023, A&A, 678, A158
Astropy Collab., Price-Whelan, A. M., SipHocz, B. M., et al. 2018, AJ, 156, 123
Astropy Collab., Robitaille, T. P., Tollerud, E. J., et al. 2013, A&A, 558, A33
Badenes, C., Mazzola, C., Thompson, T. A., et al. 2018, ApJ, 854, 147
Beck, P. G., Bedding, T. R., Mosser, B., et al. 2011, Science, 332, 205
Beck, P. G., Grossmann, D. H., Steinwender, L., et al. 2024, A&A, 682, A7
Beck, P. G., Kallinger, T., Pavlovski, K., et al. 2018a, A&A, 612, A22
Beck, P. G., Masseron, T., Pablovski, K., et al. 2025, in preparation
Beck, P. G., Mathis, S., Gallet, F., et al. 2018b, MNRAS, 479, L123
Beck, P. G., Mathur, S., Hambleton, K., et al. 2022, A&A, 667, A31
Beck, P. G., Montalban, J., Kallinger, T., et al. 2012, Nature, 481, 55
Bedding, T. R., Mosser, B., Huber, D., et al. 2011, Nature, 471, 608
Belokurov, V., Penoyre, Z., Oh, S., et al. 2020, MNRAS, 496, 1922
Benbakoura, M., Gaulme, P., McKeever, J., et al. 2021, A&A, 648, A113
Bildsten, L., Paxton, B., Moore, K., & Macias, P. J. 2012, ApJ, 744, L6
Borucki, W. J., Koch, D., Basri, G., et al. 2010, Science, 327, 977
Brown, T. M., Gilliland, R. L., Noyes, R., & Ramsey, L. 1991, ApJ, 368, 599
Cantat-Gaudin, T., Fouesneau, M., Rix, H.-W., et al. 2023, A&A, 669, A55
Castro-Ginard, A., Anders, F., Jordi, C., et al. 2023, A&A, 677, A37
Chaplin, W. J., Kjeldsen, H., Christensen-Dalsgaard, J., et al. 2011, Sci, 332, 213
Chaplin, W. J. & Miglio, A. 2013, ARA&A, 51, 353
Choi, J. Y., Espinoza-Rojas, F., Coppée, Q., & Hekker, S. 2025, arXiv e-prints, arXiv:2506.01745
Creevey, O. L., Metcalfe, T. S., Schultheis, M., et al. 2017, A&A, 601, A67
del Burgo, C. & Allende Prieto, C. 2018, MNRAS, 479, 1953
Dewberry, J. W. & Wu, Y. 2025, arXiv: 2501.13929
Dréau, G., Mosser, B., Lebreton, Y., Gehan, C., & Kallinger, T. 2021, A&A, 650, A115
Eggleton, P. P. 1983, ApJ, 268, 368
El-Badry, K., Lam, C., Holl, B., et al. 2024, OJAp, 7, 100
Escorza, A., Siess, L., Van Winckel, H., & Jorissen, A. 2020, A&A, 639, A24
Esseldeurs, M., Mathis, S., & Decin, L. 2024, A&A, 690, A266
Gaia Collaboration, Arenou, F., Babusiaux, C., et al. 2023a, A&A, 674, A34
Gaia Collaboration, Prusti, T., de Bruijne, J. H. J., et al. 2016, A&A, 595, A1
Gaia Collaboration, Vallenari, A., Brown, A. G. A., et al. 2023b, A&A, 674, A1
Gallet, F., Charbonnel, C., Amard, L., et al. 2017, A&A, 597, A14
Gaulme, P., Jackiewicz, J., Appourchaux, T., & Mosser, B. 2014, ApJ, 785, 5
Gaulme, P., McKeever, J., Jackiewicz, J., et al. 2016, ApJ, 832, 121
Ge, J., Zhang, H., Zang, W., et al. 2022, arXiv: 2206.06693
Ginsburg, A., Sipőcz, B. M., Brasseur, C. E., et al. 2019, AJ, 157, 98
Godoy-Rivera, D., Mathur, S., García, R. A., et al. 2025, A&A, 696, A243
Grossmann, D. H., Beck, P. G., Mathur, S., et al. 2025, A&A, 696, A42
Halbwachs, J.-L., Pourbaix, D., Arenou, F., et al. 2023, A&A, 674, A9
Han, Z., Podsiadlowski, P., Maxted, P. F. L., Marsh, T. R., & Ivanova, N. 2002, MNRAS, 336, 449
Harris, C., Millman, K., van der Walt, S., et al. 2020, Nature, 585, 357–362
Hekker, S., Angelou, G. C., Elsworth, Y., & Basu, S. 2020, MNRAS, 492, 5940
Hjellming, M. S. & Webbink, R. F. 1987, ApJ, 318, 794
Houdek, G. & Dupret, M.-A. 2015, Living Reviews in Solar Physics, 12, 8
Howell, S. B., Sobeck, C., Haas, M., et al. 2014, PASP, 126, 398
Huber, D., Pinsonneault, M., Beck, P., et al. 2023, arXiv: 2307.03237
Hunter, J. D. 2007, Computing in Science Engineering, 9, 90
Ivanova, N., Justham, S., Chen, X., et al. 2013, A&A Rev., 21, 59
Jones, D. & Boffin, H. M. J. 2017, Nature Astronomy, 1, 0117
Jørgensen, A. C. S., Montalbán, J., Miglio, A., et al. 2020, MNRAS, 495, 4965
Kallinger, T., Mosser, B., Hekker, S., et al. 2010, A&A, 522, A1
Katz, D., Sartoretti, P., Cropper, M., et al. 2019, A&A, 622, A205
Katz, D., Sartoretti, P., Guerrier, A., et al. 2023, A&A, 674, A5
Kepler, J. 1619, Harmonices mvndi
Kilic, M., Bergeron, P., Blouin, S., et al. 2025, ApJ, 979, 157
Kippenhahn, R., Weigert, A., & Weiss, A. 2013, Stellar Structure and Evolution
Kjeldsen, H. & Bedding, T. R. 1995, A&A, 293, 87
Kochanek, C. S., Adams, S. M., & Belczynski, K. 2014, MNRAS, 443, 1319
Lada, C. J. 2006, ApJ, 640, L63
Lam, C., El-Badry, K., Holl, B., et al. 2024 [arXiv:2411.00654]
Majewski, S. R., Schiavon, R. P., Frinchaboy, P. M., et al. 2017, AJ, 154, 94
Mathis, S. 2015, A&A, 580, L3
Mathur, S., García, R. A., Breton, S., et al. 2022, A&A, 657, A31
Mathur, S., García, R. A., Bugnet, L., et al. 2019, FrASS, 6, 46
Mazzi, A., Thomsen, J. S., Miglio, A., et al. 2025, arXiv:2504.19866
Merc, J., Beck, P. G., Mathur, S., & García, R. A. 2024, A&A, 683, A84
Miglio, A., Brogaard, K., Stello, D., et al. 2012, MNRAS, 419, 2077
Miglio, A., Chaplin, W. J., Farmer, R., et al. 2014, ApJL, 784, L3
Mirouh, G. M., Hendriks, D. D., Dykes, S., Moe, M., & Izzard, R. G. 2023, MNRAS, 524, 3978
Moe, M. & Di Stefano, R. 2017, ApJS, 230, 15
Mosser, B., Benomar, O., Belkacem, K., et al. 2014, A&A, 572, L5
Mosser, B., Elsworth, Y., Hekker, S., et al. 2012, A&A, 537, A30
Nelemans, G., Preece, H., Temmink, K., Munday, J., & Pols, O. 2025, arXiv e-prints, arXiv:2506.16832
Offner, S. S. R., Moe, M., Kratter, K. M., et al. 2023, 534, 275
Ogilvie, G. I. 2013, MNRAS, 429, 613
Ogilvie, G. I. & Lin, D. N. C. 2007, ApJ, 661, 1180
Oliphant, T. 2006, NumPy: A guide to NumPy, USA: Trelgol Publishing
Patrick, L. R., Lennon, D. J., Najarro, F., et al. 2025, A&A, 698, A39
Patton, R. A., Pinsonneault, M. H., Cao, L., et al. 2024, MNRAS, 528, 3232
Pinsonneault, M. & Ryden, B. 2023, Stellar Structure and Evolution
Pinsonneault, M. H., Elsworth, Y., Epstein, C., et al. 2014, ApJS, 215, 19
Pinsonneault, M. H., Elsworth, Y. P., Tayar, J., et al. 2018, ApJS, 239, 32
Pinsonneault, M. H., Zinn, J. C., Tayar, J., et al. 2025, ApJS, 276, 69
Podsiadlowski, P. 2001, in ASP Conf. Ser, Vol. 229, Evolution of Binary and Multiple Star Systems, 239
Pourbaix, D., Tokovinin, A. A., Batten, A. H., et al. 2004, A&A, 424, 727
Raghavan, D., McAlister, H. A., Henry, T. J., et al. 2010, ApJS, 190, 1
Rauer, H., Aerts, C., & the Plato Mission Consortium. 2024, arXiv: 2406.05447
Rauer, H., Catala, C., Aerts, C., et al. 2014, Experimental Astronomy, 38, 249
Ricker, G. R., Winn, J. N., Vanderspek, R., et al. 2014, in SPIE 914320, 914320
Salaris, M. & Cassisi, S. 2005, Evolution of Stars and Stellar Populations
Schimak, L. S., Bedding, T., Crawford, C., et al. 2025, MNRAS (submitted)
Sekaran, S., Johnston, C., Tkachenko, A., et al. 2019, A&A, 624, A140
Serenelli, A., Weiss, A., Aerts, C., et al. 2021, A&A Rev., 29, 4
Serenelli, A., Weiss, A., Cassisi, S., Salaris, M., & Pietrinferni, A. 2017, A&A, 606, A33
Skumanich, A. 1972, ApJ, 171, 565
Soberman, G., Phinney, E., & van den Heuvel, E. 1997, A&A, 327, 620
Thomsen, J. S., Miglio, A., Brogaard, K., et al. 2025, arXiv e-prints, arXiv:2504.17853
Torres, G., Andersen, J., & Giménez, A. 2010, A&A Rev., 18, 67
Van Rossum, G. & Drake, F. L. 2009, Python 3 Ref. Man. (Scotts Valley, CA)
Virtanen, P., Gommers, R., Oliphant, T. E., et al. 2020, Nature Methods, 17, 261
Vos, J., Bobrick, A., & Vučković, M. 2020, A&A, 641, A163
Vrard, M., Pinsonneault, M. H., Elsworth, Y., et al. 2024, arXiv: 2411.03101
Warfield, J. T., Zinn, J. C., Schonhut-Stasik, J., et al. 2024, AJ, 167, 208
Wolniewicz, L. M., Berger, T. A., & Huber, D. 2021, AJ, 161, 231
Zahn, J.-P. 1977, A&A, 57, 383
Zahn, J.-P. 1989, A&A, 220, 112
Zahn, J.-P. 2013, in Lecture Notes in Physics, Vol. 861, 301, 301
Zahn, J.-P. & Bouchet, L. 1989, A&A, 223, 112
Zinn, J. C. 2021, AJ, 161, 214
Zinn, J. C., Stello, D., Elsworth, Y., et al. 2022, ApJ, 926, 191